

Realizing effective magnetic field for photons by controlling the phase of dynamic modulation

Kejie Fang¹, Zongfu Yu² and Shanhui Fan^{2*}

The goal to achieve arbitrary control of photon flow has motivated much of the recent research on photonic crystals and metamaterials. As a new mechanism for controlling photon flow, we introduce a scheme that generates an effective magnetic field for photons. We consider a resonator lattice in which the coupling constants between the resonators are harmonically modulated in time. With appropriate choice of the spatial distribution of the modulation phases, an effective magnetic field for photons can be created, leading to a Lorentz force for photons and the emergence of topologically protected one-way photon edge states that are robust against disorders—without the use of magneto-optical effects.

For charged particles such as electrons, the use of a magnetic field has played an essential role in many fundamental physical phenomena and applications. On the classical level, a Lorentz force induced by a magnetic field has been used to create devices such as magnetic lenses, which are widely used in modern accelerators and electron microscopy. On the quantum level, when a low-temperature two-dimensional electron gas is placed in a perpendicular magnetic field, the transverse conductance of the electron gas becomes quantized, leading to integer and fractional quantum Hall effects^{1,2}. One defining property of quantum Hall systems is the existence of unidirectional edge modes^{3,4}, which are topologically protected and characterized by a non-zero Chern number for the bulk band structure^{5,6}.

Photons are neutral particles. Accordingly, there are no naturally analogous magnetic fields. Nevertheless, with the development of artificial photonic structures such as photonic crystals^{7–9} and metamaterials^{10–12}, there has been considerable interest recently in seeking to manipulate photons in a manner similar to the manipulation of electrons using a magnetic field. In particular, an effective magnetic field in *momentum* space for photons has been discussed extensively, and has been used to achieve the Hall effect for light¹³ and to realize one-way edge modes in magneto-optical photonic crystal that are direct photonic analogues of quantum Hall systems^{14–18}. These achievements, however, do not correspond directly to a magnetic field in *real* space.

An optical analogue of the quantum spin Hall effect has also been proposed^{19,20}. In such systems, photons with opposite spins experience an effective magnetic gauge field along opposite directions. As a result, the edge modes of opposite spins propagate in opposite directions, therefore realizing a photonic analogue of the electronic quantum spin Hall effect. However, the gauge field in these systems does not break time-reversal symmetry.

For photons, in contrast to electrons, there is no Kramers degeneracy. Consequently, unlike a regular electronic potential perturbation, which preserves electron spin²¹, a regular dielectric perturbation in photonics typically induces photon spin mixing. As a result, the edge modes in refs 19 and 20 are not robust against all disorders. Such a limitation has been noted in experiments on systems that exhibit similar spin-dependent photon dispersion relations²².

In a recent paper²³, it was shown that in interband photonic transitions, as induced by dynamic refractive index modulation, the

phase of the modulation is connected to a gauge transformation of the photon wavefunction. In ref. 23, this effect was then used to construct an optical isolator. An effective magnetic field, however, is characterized by the highly non-trivial topological properties of photon wavefunctions. In two dimensions, for example, one such topological property is a non-zero Chern number. Such a topological property is absent in most isolators (which are one-dimensional systems), including the isolator of ref. 23. Here, we show that, by specifically configuring a system undergoing interband photonic transition, we can naturally achieve an effective magnetic field that couples to photons. Such an effective magnetic field breaks time-reversal symmetry and operates in *real* space. As demonstrations, we show that such an effective magnetic field can lead to the circular motion of light beams, as driven by a Lorentz-like force, and photonic one-way edge modes in a photonic resonator lattice.

Effective magnetic field

To introduce an effective magnetic field for photons we consider a square lattice of photonic resonators as shown in Fig. 1. The lattice consists of two interpenetrating square sublattices, labelled A and B. The resonators in each sublattice have frequencies of ω_A and ω_B , respectively. We assume only nearest-neighbour coupling, and the coupling occurs only between the two sublattices. Moreover, we assume that the coupling constants are modulated harmonically^{24–26}. We will discuss physical implementations that achieve such a coupling in the section ‘Proposal for experimental implementation’. The resulting Hamiltonian is then given by

$$H = \omega_A \sum_i a_i^\dagger a_i + \omega_B \sum_j b_j^\dagger b_j + \sum_{\langle ij \rangle} V \cos(\Omega t + \phi_{ij})(a_i^\dagger b_j + b_j^\dagger a_i) \quad (1)$$

where V is the strength of the coupling, Ω is the modulation frequency, ϕ_{ij} is the phase of the modulation between resonators at sites i and j , and a_i^\dagger and b_j^\dagger are the creation operators in the A and B sublattices, respectively. In this system, the modulation is therefore applied on the ‘bonds’ that connect sites i and j .

We now assume in Hamiltonian (1) that $\Omega = \omega_A - \omega_B$, and V much less than symbol Ω . In this limit, the rotating wave

¹Department of Physics, Stanford University, Stanford, California 94305, USA, ²Department of Electrical Engineering, Stanford University, Stanford, California 94305, USA. *e-mail: shanhui@stanford.edu

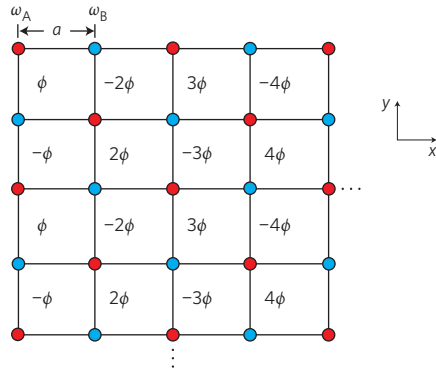


Figure 1 | Dynamically modulated photonic resonator lattice exhibiting an effective magnetic field for photons. A lattice of photonic resonators, with two square sublattices of resonators with frequency ω_A (red) and ω_B (blue), respectively. There is only nearest-neighbour dynamic coupling. The phase of the dynamic coupling on the horizontal bonds is zero. The phase on the vertical bonds is proportional to the column index, and within the same column the sign is flipped between two neighbouring bonds.

approximation can be applied and, as a result, in the rotating frame the Hamiltonian simplifies to

$$H = \sum_{\langle ij \rangle} \frac{V}{2} (e^{-i\phi_{ij}} c_i^\dagger c_j + e^{i\phi_{ij}} c_j^\dagger c_i) \quad (2)$$

where $c_{i(j)} = e^{i\omega_{A(B)}t} a_i(b_j)$. Hamiltonian (2) is identical to the Hamiltonian of a charged particle on a lattice subjected to a magnetic field²⁷, if we make the association

$$\int_i^j \mathbf{A}_{\text{eff}} d\mathbf{l} = \phi_{ij} \quad (3)$$

Thus, we find that the phase of the harmonic modulation can introduce an effective gauge potential \mathbf{A}_{eff} to photons. The phase distribution of Fig. 1 corresponds to the Landau gauge in the rotating

frame, as photons hopping along the positive y -direction at a given x -coordinate always acquire the same phase.

To achieve a uniform effective magnetic field for photons, we assigned the modulation phase shown in Fig. 1, with all bonds along the x -direction having the same phase 0, and each bond along the y -direction having a different modulation phase, depending on the location of the bond. Under a phase distribution such as that in Fig. 1, the lattice is associated with a uniform effective magnetic field B_{eff} ,

$$B_{\text{eff}} = \frac{1}{a^2} \oint_{\text{plaquette}} \mathbf{A}_{\text{eff}} d\mathbf{l} = \frac{\phi}{a^2} \quad (4)$$

where a is the lattice constant.

From the analytic arguments in equations (2) to (4), we therefore see that the modulation phase in the time-dependent Hamiltonian in equation (1) can be used to achieve an effective magnetic field for a photon. Below, we will verify this prediction by a direct numerical simulation of the time-dependent Hamiltonian in equation (1), and by demonstrating some of the novel electromagnetic effects associated with the presence of an effective magnetic field.

Lorentz force

Classically, in free space, a particle of charge q and mass m in a uniform magnetic field \mathbf{B} is driven by the Lorentz force, $\mathbf{F} = q\mathbf{v} \times \mathbf{B}$, where \mathbf{v} is the velocity of the charged particle. As a result, the charged particle moves in a circle in a plane perpendicular to the uniform magnetic field, with radius $R = mv/(qB)$, if the initial velocity \mathbf{v} is perpendicular to the magnetic field. The same circular motion can also be observed quantum mechanically if one considers the motion of a wave packet of the charged particle subject to a magnetic field.

We now show that the effective magnetic field, as introduced by the choice of modulation phase distribution, can also induce a circular motion of a photon wavepacket. We consider the structure shown in Fig. 2a. The right half of the lattice has a phase distribution as in Fig. 1, representing a uniform effective magnetic field B_{eff} as given by equation (4). The left half of the lattice has modulation phase $\phi_{ij} = 0$ for any i, j , which represents a region free of effective

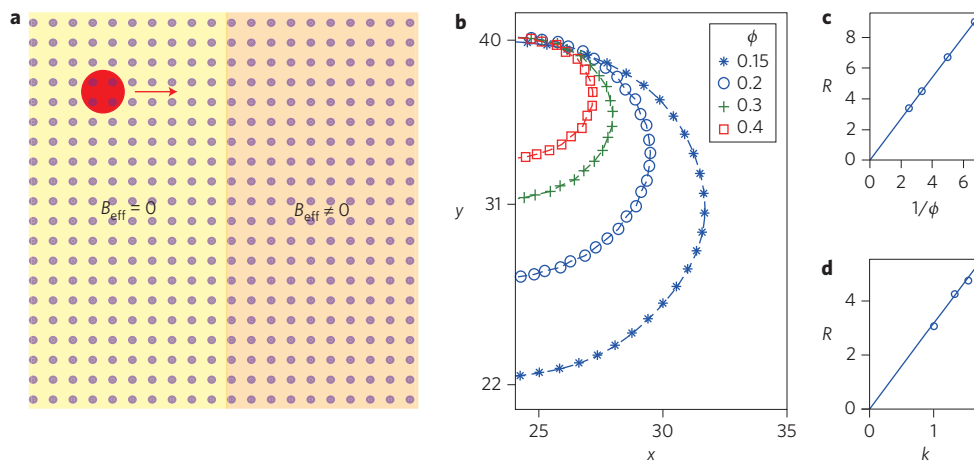


Figure 2 | Photon motion in an effective magnetic field. **a**, Structure (part), comprising the resonator lattice shown in Fig. 1, used to demonstrate the Lorentz force for photons. Resonators are indicated by dots. Lattice parameters: $\omega_A = 30$, $\omega_B = 0$, $\Omega = 0$, $V = 6$ (all in units of $2\pi c/a$). The left part of the lattice has no effective magnetic field ($\phi = 0$). The right part of the lattice has an effective magnetic field with the modulation phase set in a pattern according to Fig. 1. A Gaussian wave packet is initiated in the left part of the structure. The packet is described by equation (5), with $w = \sqrt{10} a$. **b**, Trajectory of the centre of mass of the wave packet, after the wave packet (with $k = -1.283/a$) has entered the right part, where an effective magnetic field is present. Different symbols correspond to different ϕ . The wave packet has a circular trajectory. **c**, Radius of the trajectory as a function of $1/\phi$ for $k = -1.283/a$. **d**, Radius of the trajectory as a function of k , for $\phi = 0.3$.

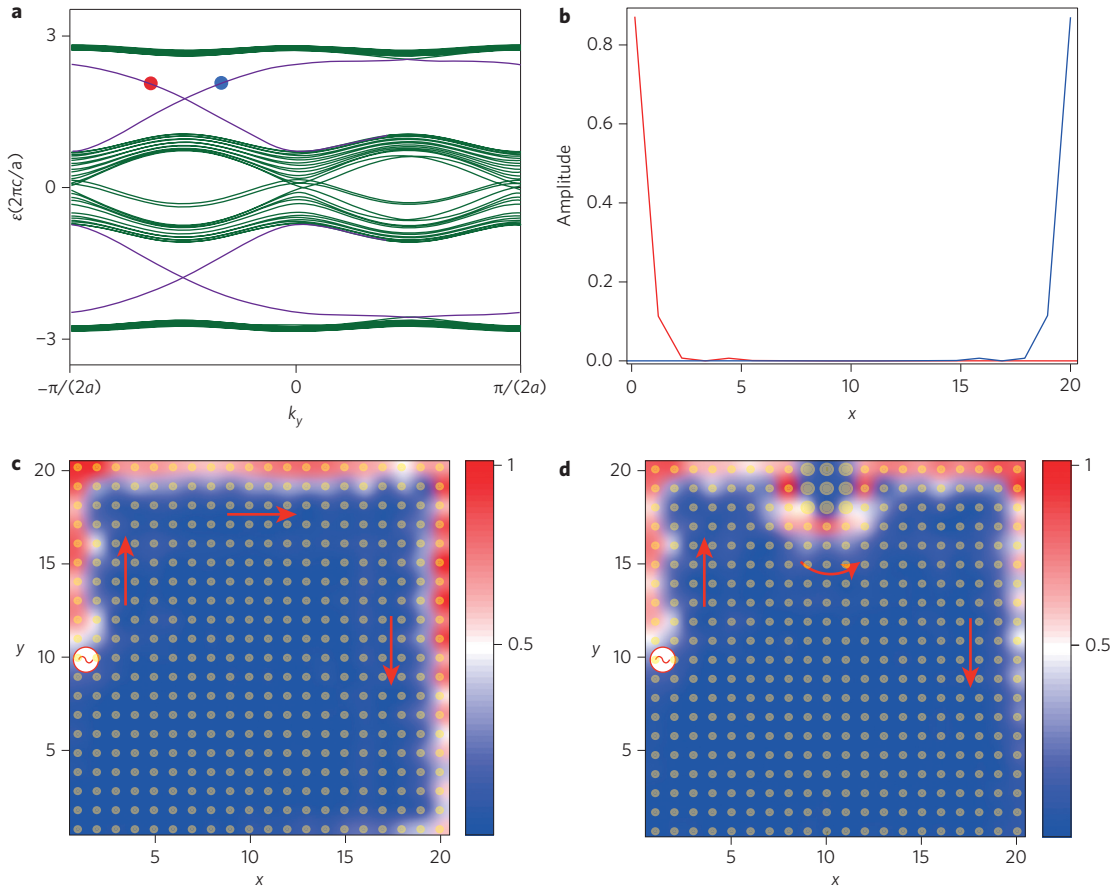


Figure 3 | Photonic one-way edge mode in a dynamically modulated resonator lattice. **a**, Projected Floquet band structure for a strip of the resonator lattice shown in Fig. 1. The strip is infinite along the y -axis, and has a width of $20a$ along the x -axis. The projection direction is along the y -axis. Parameters of the lattice: $\phi = \pi/2$, $\omega_A = 100$, $\omega_B = 0$, $\Omega = 100$, $V = 2$ (all in units of $2\pi c/a$). There are four separate groups of bulk bands (green curves, the centre two bands do not split). In each bandgap between the bulk bands there are two one-way edge modes, which are located on the two edges of the strip. **b**, Field amplitude of the two edge modes indicated by red and blue dots in **a**. The fields are located on the two edges and decay exponentially into the bulk. **c**, Propagation of one-way edge modes. We consider a 20×20 lattice of resonators as shown in Fig. 1 (resonators are indicated as yellow dots), and excite the edge mode by locating a point source with $\omega_s = 2(2\pi c/a)$ at the position indicated by the red marker. The field profile at time $t = 40(a/2\pi c)$ is plotted. The propagation of the edge mode is unidirectional. **d**, Propagation of the one-way edge mode in the presence of a defect. The defect is a 3×3 sublattice of resonators with frequency $\omega_d = 50(2\pi c/a)$ for each resonator, as indicated by the larger yellow dots. All other parameters are as in **c**. Notice that the edge mode propagates around the defect, indicating one-way propagation robust against defect.

magnetic field. At $t = 0$, we initiate the system such that the photon is described by a wave packet of the form

$$\psi = e^{-((x-x_0)^2 + (y-y_0)^2)/w^2} e^{ikx} \quad (5)$$

This wave packet has a Gaussian amplitude profile centering at (x_0, y_0) with waist w , and an average Bloch wavevector $k\hat{x}$. In the region free of magnetic field, the wave packet moves with a group velocity v_g towards the region with an effective magnetic field.

In Fig. 2b we plot the trajectory of the centre of mass (\mathbf{r}) of the wave packet. On entering the region with an effective magnetic field, the packet indeed follows a circular trajectory. Moreover, as we decrease the modulation phase ϕ in Fig. 1, which corresponds to a decrease in the effective magnetic field, the radius of the circular motion increases (Fig. 2b,c). Also, at the same effective magnetic field (that is, the same ϕ), the radius increases as a function of k . Quantitatively, the radius of the circular motion is perfectly described by

$$R = \frac{k}{\phi} \quad (6)$$

Equations (6), for photons, is a counterpart to the formula for charged particles, as the Bloch momentum k of the photons replaces momentum mv of the charged particles, and effective magnetic field $B_{\text{eff}} = \phi$ (we set $a = 1$) replaces qB . equation (6) is a direct result of an effective Lorentz force $\mathbf{F}_{\text{Lorentz}} = \mathbf{v}_g \times \phi \hat{z}$ acting on photons, where v_g is the group velocity of the photon wave packet.

Similar to the circular motion of a charged particle in a magnetic field, the photon motion here is non-reciprocal. With this choice of modulation phase distribution, the photon wave packet will always follow a circular trajectory in a clockwise direction, independent of the direction of the wave packet velocity.

One-way edge mode

The spectrum of a two-dimensional electron gas in a square lattice in the presence of a perpendicular uniform magnetic field is described as ‘Hofstadter’s butterfly’²⁸. If the magnetic flux through a unit cell is rational, that is, $eBa^2/(hc) = m/n$, where a is the lattice constant, h is Planck’s constant and c is the speed of light, with m and n relatively prime, the spectrum has n bands. Unidirectional edge modes can exist in the gap between the bands⁶.

We show that the dynamically modulated photonic resonator lattice in Fig. 1 also supports one-way edge modes. For the

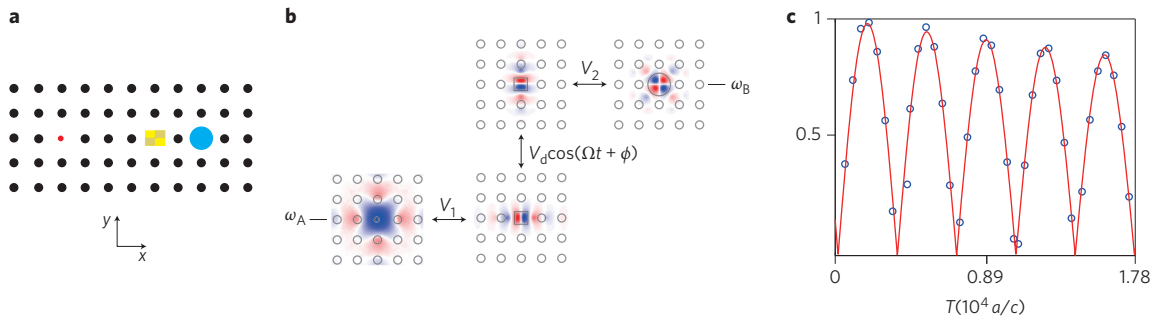


Figure 4 | Dynamic coupling between photonic-crystal resonators. **a**, A photonic crystal made from dielectric rods (black) with a permittivity of 8.9 and radius of $0.2a$ (a is the lattice constant). The resonator on the left (red) is a rod with permittivity of 7.4 and radius of $0.12a$, and is shifted $0.04a$ to the left from the lattice point. Such a resonator supports a monopole mode. The resonator on the right (blue) is a rod with permittivity of 9.1 and radius of $0.56a$. It supports a quadrupole- xy mode. The resonator in the middle (yellow and brown) is a rectangular rod with permittivity of 8.9 and side lengths of $0.66a$ and $0.62a$ along the x -axis and y -axis, respectively. It supports a pair of split dipole modes. With these chosen parameters, the frequency of the monopole mode and p_x mode have the same frequency of $0.346(2\pi c/a)$, and the quadrupole mode and p_y mode have the same frequency of $0.352(2\pi c/a)$. The static coupling strength within each two equal-frequency pair is also similar. Dynamic modulation with $\Omega = 0.006(2\pi c/a)$ and permittivity modulation $\Delta\epsilon = 0.002$ is applied on the middle resonator. The modulation has a quadrupolar profile, with the modulation in the first and third quadrants (brown) and the modulation in the second and fourth quadrant (yellow) having a π phase difference. **b**, Electric field (along the z -axis) of the four resonant states, and the scheme of generating dynamic coupling between the monopole and quadrupole. **c**, The amplitude envelope of the monopole mode as a function of time when the quadrupole mode is initially excited, for the structure in **a**. Circles are data from finite-difference time-domain simulations. Red curve is the solution of the coupled mode equations describing the effective coupling between two resonant states.

dynamically modulated lattice, because the Hamiltonian is temporally periodic, one can apply the concepts of Floquet band structure and quasi-energy to illustrate its spectrum^{29,30}. For a temporally periodic system with Hamiltonian $H(t + T) = H(t)$, its state is described by a wavefunction of the Floquet form in time $\psi(t) = e^{-i\epsilon t}\Phi(t)$, where ϵ is the quasi energy. $\Phi(t)$ is a periodic function, that is, $\Phi(t + T) = \Phi(t)$, which satisfies an eigenvalue equation $(H(t) - i\partial_t)\Phi(t) = \epsilon\Phi(t)$. By decomposing $\Phi(t)$ in Fourier space consisting of the harmonics of multiple $2\pi/T$, the eigenvalue equation can be converted into a matrix form and be solved numerically, providing a method for obtaining the quasi energy ϵ . In a temporally periodic system that also has spatial periodicity, one can calculate the quasi energy ϵ for states with different wavevectors to obtain the Floquet band structure.

Using this method, we calculated the Floquet band structure of the dynamically modulated square lattice of resonators in Fig. 1. For the phase distribution we chose, the system is periodic along the y -direction with period $2a$, and thus k_y is still a good quantum number. We consider a strip that has 20 lattice sites along the x -direction and an infinite number along the y -direction, and plot the projected Floquet band structure in terms of the quasi energy ϵ as a function of k_y . As an example, for $\phi = \pi/2$, corresponding to an effective magnetic flux of $1/4$, the Floquet band structure is shown Fig. 3a. The bulk band structure indeed splits into four groups of bands, consistent with the description of the band structure in terms of Hofstadter’s butterfly. In the bandgaps, for each edge, there is a one-way edge mode, with field amplitude decaying exponentially into the bulk (Fig. 3b).

We simulated the propagation of the edge mode in a 20×20 lattice with the same parameters as above. We placed a point source with frequency $\omega_s = 2(2\pi c/a)$ on one side of the square lattice to excite the edge mode. We see that the edge mode propagates unidirectionally along the boundary of the square lattice (Fig. 3c). Because the lattice is associated with a uniform effective magnetic field, a one-way edge mode also appears on the edges parallel to the x -axis, even though, due to the lack of translational symmetry along the x -axis in the particular phase distribution that we have chosen, one cannot define a projected band structure along the x -axis. This edge mode is robust against defects on the edge. To demonstrate this, we changed the frequency of the resonators

in a 3×3 sublattice on the top side of the square lattice to $\omega_d = 50(2\pi c/a)$. In this case, the edge mode can go around the defect sublattice and maintain unidirectional propagation (Fig. 3d). We have therefore demonstrated the existence of a one-way edge mode that is robust against disorders in this dynamically modulated lattice.

Achieving a one-way edge mode is of great importance to optical and electromagnetic technology, because it offers protection against fabrication-related disorders. To date, all proposed mechanisms for achieving a one-way edge mode rely on magneto-optical effects, which are difficult to achieve in on-chip implementations^{14–18}. Although spin-dependent one-way edge modes have been discussed in refs 19 and 22, the structures in those references do not break time-reversal symmetry and hence do not provide complete immunity to disorder-induced backscattering. Because dynamic modulation is readily achievable on-chip^{31,32}, our work suggests a route towards the on-chip demonstration and application of such topologically protected photonic states.

Proposal for experimental implementation

In this section we discuss the physical implementation of Hamiltonian (1). To implement this Hamiltonian requires one to harmonically modulate the coupling constant between two spatially separated resonators. We will discuss mechanisms to achieve such a dynamic coupling at both optical and microwave frequencies. In both cases, a key requirement is that the strength of the dynamic coupling V should be larger than the decay rate γ of the resonators, such that a photon wave packet can propagate over a considerable distance in the modulated lattice before it is damped.

In the optical regime, we consider a photonic-crystal resonator lattice. An example of the lattice structure showing only two resonators is shown in Fig. 4a. Here, we aim to achieve a dynamic coupling between a resonator on the left (red, Fig. 4a) and a resonator on the right (blue, Fig. 4a). The left resonator supports a monopole at frequency ω_A , and the right resonator supports a quadrupole- xy mode at frequency ω_B (Fig. 4b)³³. These two modes have different symmetry with respect to the mirror planes parallel to the x -axis and y -axis to prevent static coupling between them.

To achieve dynamic coupling between these two resonators, we introduced an intermediate resonator between them (yellow, Fig. 4a).

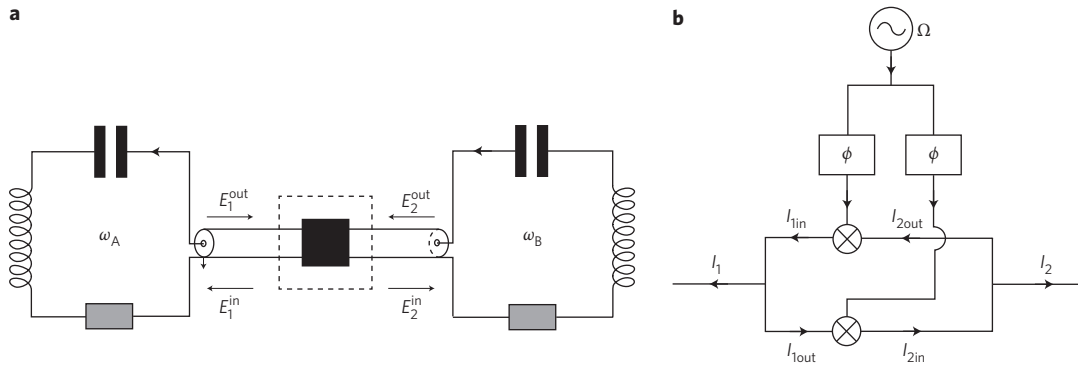


Figure 5 | Realization of dynamic coupling between resonators in the microwave regime. a, Two microwave RLC resonators with frequencies ω_A and ω_B , respectively, coupled through a transmission line waveguide incorporating a frequency conversion device. The frequency conversion device introduces dynamic coupling between the resonators. **b**, Circuit implementation of the frequency conversion device in **a**. The device is composed of two mixers (circled cross) in parallel, which are biased with opposite d.c. voltages such that the current only flows in one direction for each mixer. The phase of the local oscillator in the mixer is ϕ , which is used to implement the phase of dynamic coupling between the two microwave resonators.

This intermediate resonator supports a p_x state with frequency ω_A , and a p_y state with frequency ω_B (Fig. 4b). The p_x state couples with the monopole at the left with strength V_1 and the p_y state couples with the quadrupole on the right with strength V_2 . A photonic transition was driven between the p_x and p_y states by modulating the refractive index of the intermediate region at frequency $\Omega = |\omega_A - \omega_B|$ (refs 24–26). Such a modulation couples the p_x and p_y state with a dynamic coupling constant $V_d \cos(\Omega t + \phi)$, where ϕ is the modulation phase that we control. In the regime where V_d much less than symbol V_1 and V_2 , which is the experimentally relevant regime because the modulation is typically weak, we can show, using coupled mode theory, that the modulation induces a dynamic coupling between the left and right resonators, with an equivalent strength of $(V_d/2) \cos(\Omega t + \phi)$ (Supplementary Section SI).

We verified the existence of dynamic coupling between the left and right resonators by a direct finite-difference time-domain simulation of the structure shown in Fig. 4a. We used a modulation strength of $\Delta\varepsilon = 0.0178$ in the intermediate region. Figure 4c shows the slowly varying envelope of the amplitude of the monopole state. A dynamic and complete Rabi oscillation clearly exists, which matches well with two-mode coupled mode theory. Thus, using first-principles simulations, we have demonstrated dynamic coupling of two spatially separated resonators.

To demonstrate the predicted effects here, the dynamic coupling strength between the resonators needs to dominate over the resonator loss rate. In the optical domain, choosing a modulation strength of $\Delta\varepsilon/\varepsilon = 5.4 \times 10^{-5}$, and a modulation frequency of $\Omega = 20$ GHz, both of which are achievable experimentally^{31,32}, we should be able to achieve a dynamic coupling strength of $V = 5 \times 10^{-5} (2\pi c/a)$, which corresponds to 14.3 GHz if we operate at a wavelength of $1.55 \mu\text{m}$, and is one order of magnitude larger than the intrinsic decay rate of state-of-the-art photonic-crystal resonators^{34,35}. In the meantime, we have $V < \Omega$ and thus the rotating wave approximation is still satisfied. Moreover, the radiation loss of resonators can in principle be removed by placing the photonic resonators in a three-dimensional photonic crystal³⁶. For this purpose, we note significant recent progress in fabricating high-quality three-dimensional photonic crystals³⁷.

To construct our system requires the integration of a substantial number of modulators on-chip, and in this regard we note a recent work demonstrating electrically induced non-reciprocity by separately modulating 88 different regions on a silicon chip³⁸. This experiment achieved a refractive index modulation of $\sim 1 \times 10^{-4}$ in each modulated region, with a total power consumption of 316 mW

(25 dBm). The predicted effects here will require a similar number of modulated regions. However, in our system, the area of each modulated region, being a single-mode resonator, can be considerably smaller than that of ref. 38 and as a result the total required electric power may be significantly lower. Finally, ref. 38 experimentally showed that the phase of the modulations can be controlled to a sufficient accuracy to achieve a significant non-reciprocal response. We believe that the requirement for phase accuracy in our design is similar.

In the microwave regime, we propose the structure shown in Fig. 5, where two RLC resonators, each having different frequencies ω_A and ω_B , are connected by transmission lines through a frequency conversion device composed of mixers. The mixer contains a local oscillator at a frequency of $\Omega = \omega_A - \omega_B$ (Fig. 5b). An incident wave from the left (right), at a frequency ω_A (ω_B), mixes with the local oscillator, and generates an output at ω_B (ω_A) to the right (left), and thus achieves dynamic coupling $V \cos(\Omega t + \phi)$ between the two resonators. The phase of the local oscillator ϕ is the modulation phase of the coupling constant between the two resonators. The strength of the coupling between the microwave resonators is $V = [2\alpha/(1 + \alpha^2)](Z_c/L)$, where L is the inductance of the microwave resonator, Z_c is the characteristic impedance of the transmission line, and α is the conversion efficiency of the mixer (Supplementary Section SII). Typical mixers have a conversion efficiency of 4–7 dB (ref. 39). Strong dynamic coupling between microwave resonators can be achieved by choosing a low resistance for the resonator. For example, for a mixer with a conversion efficiency of 4 dB, the resistance R of the microwave resonator should satisfy $R < 1.37Z_c$ (typically $Z_c = 50 \Omega$), to meet the requirement $V > \gamma$.

In summary, we have shown that in a dynamically modulated photonic resonator lattice, the modulation phases introduce a gauge field for photons, which can be used to apply an effective magnetic field to the photons. Here, for illustration purposes, we have considered only a uniform effective magnetic field. However, because the modulation phase distributions can be arbitrarily specified, we anticipate tremendous richness of photon motion in such a dynamic lattice, which is important for both fundamental studies and potential applications. This work should provide additional stimulus to the significant recent works aiming to achieve non-magnetic on-chip non-reciprocity^{40–43}, by highlighting new fundamental physics effects in these systems.

Received 2 April 2012; accepted 17 August 2012;
published online 7 October 2012

References

1. Klitzing, K. V., Dorda, G. & Pepper, M. New method for high-accuracy determination of the fine-structure constant based on quantized Hall resistance. *Phys. Rev. Lett.* **45**, 494–497 (1980).
2. Tsui, D. C., Stormer, H. L. & Gossard, A. C. Two-dimensional magnetotransport in the extreme quantum limit. *Phys. Rev. Lett.* **48**, 1559–1562 (1982).
3. Laughlin, R. Quantized Hall conductivity in two dimensions. *Phys. Rev. B* **23**, 5632–5633 (1981).
4. Halperin, B. I. Quantized Hall conductance, current-carrying edge states, and the existence of extended states in a two-dimensional disordered potential. *Phys. Rev. B* **25**, 2185–2190 (1982).
5. Thouless, D., Kohmoto, M., Nightingale, M. & Nijs, M. Quantized Hall conductance in a two-dimensional periodic potential. *Phys. Rev. Lett.* **49**, 405–408 (1982).
6. Hatsugai, Y. Chern number and edge states in the integer quantum Hall effect. *Phys. Rev. Lett.* **71**, 3697–3700 (1993).
7. Yablonoitch, E. Inhibited spontaneous emission in solid-state physics and electronics. *Phys. Rev. Lett.* **58**, 2059–2062 (1987).
8. John, S. Strong localization of photons in certain disordered dielectric superlattices. *Phys. Rev. Lett.* **58**, 2486–2489 (1987).
9. Joannopoulos, J. D., Villeneuve, P. R. & Fan, S. Photonic crystals: putting a new twist on light. *Nature* **386**, 143–149 (1997).
10. Pendry, J. B. Negative refraction makes a perfect lens. *Phys. Rev. Lett.* **85**, 3966–3969 (2000).
11. Smith, D. R., Pendry, J. B. & Wiltshire, M. C. K. Metamaterials and negative refractive index. *Science* **305**, 788–792 (2004).
12. Shalaev, V. M. Optical negative-index metamaterials. *Nature Photon.* **1**, 41–48 (2007).
13. Onoda, M., Murakami, S. & Nagaosa, N. Hall effect of light. *Phys. Rev. Lett.* **93**, 083901 (2004).
14. Raghun, S. & Haldane, F. D. M. Analogs of quantum-Hall-effect edge states in photonic crystals. *Phys. Rev. A* **78**, 033834 (2008).
15. Haldane, F. D. M. & Raghun, S. Possible realization of directional optical waveguides in photonic crystals with broken time-reversal symmetry. *Phys. Rev. Lett.* **100**, 013904 (2008).
16. Wang, Z., Chong, Y., Joannopoulos, J. D. & Soljačić, M. Reflection-free one-way edge modes in a gyromagnetic photonic crystal. *Phys. Rev. Lett.* **100**, 013905 (2008).
17. Wang, Z., Chong, Y., Joannopoulos, J. D. & Soljačić, M. Observation of unidirectional backscattering-immune topological electromagnetic states. *Nature* **461**, 772–775 (2009).
18. Yu, Z., Veronis, G., Wang, Z. & Fan, S. One-way electromagnetic waveguide formed at the interface between a plasmonic metal under a static magnetic field and a photonic crystal. *Phys. Rev. Lett.* **100**, 023902 (2008).
19. Hafezi, M., Demler, E. A., Lukin, M. D. & Taylor, J. M. Robust optical delay lines with topological protection. *Nature Phys.* **7**, 907–912 (2011).
20. Umucallar, R. O. & Carusotto, I. Artificial gauge field for photons in coupled cavity arrays. *Phys. Rev. A* **84**, 043804 (2011).
21. Kane, C. L. Graphene and the quantum spin Hall effect. *Int. J. Mod. Phys. B* **21**, 1155–1164 (2007).
22. Chen, W.-J. *et al.* Observation of backscattering-immune chiral electromagnetic modes without time reversal breaking. *Phys. Rev. Lett.* **107**, 023901 (2011).
23. Fang, K., Yu, Z. & Fan, S. Photonic Aharonov–Bohm effect based on dynamic modulation. *Phys. Rev. Lett.* **108**, 153901 (2012).
24. Winn, J. N., Fan, S., Joannopoulos, J. D. & Ippen, E. P. Interband transitions in photonic crystals. *Phys. Rev. B* **59**, 1551–1554 (1999).
25. Dong, P., Preble, S. F., Robinson, J. T., Maniapatruni, S. & Lipson, M. Inducing photonic transitions between discrete modes in a silicon optical microcavity. *Phys. Rev. Lett.* **100**, 033904 (2008).
26. Yu, Z. & Fan, S. Complete optical isolation created by indirect interband photonic transitions. *Nature Photon.* **3**, 91–94 (2009).
27. Luttinger, J. M. The effect of a magnetic field on electrons in a periodic potential. *Phys. Rev.* **84**, 814–817 (1951).
28. Hofstadter, D. R. Energy levels and wave functions of Bloch electrons in rational and irrational magnetic fields. *Phys. Rev. B* **14**, 2239–2249 (1976).
29. Sherry, J. H. Solution of the Schrödinger equation with a Hamiltonian periodic in time. *Phys. Rev.* **138**, B979–B987 (1965).
30. Samba, H. Steady states and quasi energies of a quantum-mechanical system in an oscillating field. *Phys. Rev. A* **7**, 2203–2213 (1973).
31. Xu, Q., Schmidt, B., Pradhan, S. & Lipson, M. Micrometre-scale silicon electro-optic modulator. *Nature* **435**, 325–327 (2005).
32. Kuo, Y.-H. *et al.* Strong quantum-confined Stark effect in germanium quantum-well structures on silicon. *Nature* **437**, 1334–1336 (2005).
33. Villeneuve, P. R., Fan, S. & Joannopoulos, J. D. Microcavities in photonic crystals: mode symmetry, tunability, and coupling efficiency. *Phys. Rev. B* **54**, 7837–7842 (1996).
34. Takahashi, Y. *et al.* High-Q nanocavity with a 2-ns photon lifetime. *Opt. Express* **15**, 17206–17213 (2007).
35. Notomi, M., Kuramochi, E. & Tanabe, T. Large-scale arrays of ultrahigh-Q coupled nanocavities. *Nature Photon.* **2**, 741–747 (2008).
36. Povinelli, M. L., Johnson, S. G., Fan, S. & Joannopoulos, J. D. Emulation of two-dimensional photonic crystal defect modes in a photonic crystal with a three-dimensional photonic band gap. *Phys. Rev. B* **64**, 075313 (2001).
37. Ishizaki, K. & Noda, S. Manipulation of photons at the surface of three-dimensional photonic crystals. *Nature* **460**, 367–370 (2009).
38. Lira, H., Yu, Z., Fan, S. & Lipson, M. Electrically driven nonreciprocity induced by interband photonic transition on a silicon chip. *Phys. Rev. Lett.* **109**, 033901 (2012).
39. Pozar, D. M. in *Microwave Engineering* Ch. 12, 618 (Wiley, 2005).
40. Koch, J., Houck, A. A., Le Hur, K. & Girvin, S. M. Time-reversal-symmetry breaking in circuit-QED-based photon lattices. *Phys. Rev. A* **82**, 043811 (2010).
41. Underwood, D., Shanks, W. E., Koch, J. & Houck, A. A. Low-disorder microwave cavity lattices for quantum simulation with photons. *Phys. Rev. A* **86**, 023837 (2012).
42. Houck, A. A., Tureci, H. E. & Koch, J. On-chip quantum simulation with superconducting circuits. *Nature Phys.* **8**, 292–299 (2012).
43. Hafezi, M. & Rabi, P. Optomechanically induced non-reciprocity in microring resonators. *Opt. Express* **20**, 7672–7684 (2012).

Acknowledgements

This work was supported in part by the US Air Force Office of Scientific Research (grant no. FA9550-09-1-0704) and the US National Science Foundation (grant no. ECCS-1201914).

Author contributions

K.F. conceived the mechanism for achieving an effective magnetic field and performed the calculations. All authors contributed to the design of the study, discussion of the results and writing of the manuscript.

Additional information

Supplementary information is available in the online version of the paper. Reprints and permission information is available online at <http://www.nature.com/reprints>. Correspondence and requests for materials should be addressed to S.F.

Competing financial interests

The authors declare no competing financial interests.